The propagation of positive streamers in a weak and uniform background electric field

Serdyuk, Y. V; Larsson, A; Gubanski, S. M; Akyuz, M

Published in:
Journal of Physics D: Applied Physics

DOI:
10.1088/0022-3727/34/4/323

2001

The propagation of positive streamers in a weak and uniform background electric field

2001 J. Phys. D: Appl. Phys. 34 614

(http://iopscience.iop.org/0022-3727/34/4/323)

INSTITUTE OF PHYSICS PUBLISHING JOURNAL OF PHYSICS D: APPLIED PHYSICS

J. Phys. D: Appl. Phys. **34** (2001) 614–623 www.iop.org/Journals/jd PII: S0022-3727(01)15818-3

The propagation of positive streamers in a weak and uniform background electric field

Yu V Serdyuk[1], A Larsson[2], S M Gubanski[1] and M Akyuz[3]

[1] Division of High Voltage Engineering, Department of Electric Power Engineering, Chalmers University of Technology, SE-412 96 Göteborg, Sweden
[2] Division of Atomic Physics and Division of Combustion Physics, Lund Institute of Technology, PO Box 118, SE-221 00 Lund, Sweden
[3] Institute of High Voltage Research, Uppsala University, Husbyborg, SE-752 28 Uppsala, Sweden

E-mail: yuriy.serdyuk@elkraft.chalmers.se

Received 26 July 2000

Abstract

The results of numerical simulations of a positive streamer development in air in a weak and uniform electric field are presented. Streamer dynamics is considered in an electrode gap of 33 mm in length and the configuration was 'protrusion on a plate–plate'. This particular configuration was chosen in order to perform direct comparison between simulated results and experimental data. The electrostatic field in such a system decreases rapidly with increase of the distance from the protrusion (anode) and the region with a weak and uniform background field covers ∼30 mm of the gap. The parameters of the propagating streamer are studied at six different values of the background field strength: 0.24; 0.30; 0.345; 0.37; 0.43 and 0.50 MV m^{-1}. Stable streamer development (with constant velocity) takes place in a field of 0.5 MV m^{-1} (the stability field) but the streamer is able to cross the gap in a background field of 0.3 MV m^{-1}. These values are in excellent agreement with experimental data. During the stable streamer propagation, the electron density and plasma conductivity in the discharge channel and the electric field at its front remain constant. In a background field lower than 0.5 MV m^{-1}, the discharge front velocity and the electric field at the front decrease linearly with an increase of streamer length. The discharge propagation in the stability field is associated with an increase of electrostatic energy at the streamer front but it decreases if the streamer develops in a weaker electric field. This behaviour is accompanied by a constant Joule dissipation at 0.5 MV m^{-1} and decreasing energy losses at the streamer front in a weaker background electric field.

1. Introduction

Electrical breakdown of air at atmospheric pressure occurs as a sequence of several processes that leads to the formation of a plasma channel which bridges the electrode gap. The main stages of an electrical breakdown in a uniform electric field are the occurrence of initial seeding electrons, the development of electron avalanches, the inception and the propagation of a streamer, the streamer-to-leader transition and, depending on the energy supply, the formation of a spark or an arc discharge. The streamer is the most critical stage of such a breakdown since it determines the characteristics and propagation ability of the electrical discharge. Furthermore, the streamer is a most complex phenomenon. Because of these reasons, the streamer mode of the discharge development is still the object of intensive experimental and theoretical studies.

A great amount of experimental results collected in the literature are devoted to integral parameters of streamer discharges under different conditions such as inception and breakdown voltages and the current in the external circuit. But it is difficult, and often even impossible, to obtain experimental data about microscopic discharge parameters

(densities and temperatures of particles of different types, distributions of charges and electric field in a gap, etc) due to the short duration of the process (of the order of tens of nanoseconds), unpredictable trajectory of propagation and low radiation from the streamer plasma. With the development of fast digital computers, theoretical studies based on numerical simulations of the discharge development have emerged. As a consequence, theoretical results are often ahead of experimental data in this respect.

The overwhelming majority of mathematical models used for streamer simulations are diffusive–drift models. Within the framework of this approach each component of the discharge plasma is treated as a Newtonian fluid. In this case, the hydrodynamic mass balance equation for each accounted species, taking into account drift, diffusion and sources of appearance and disappearance, are employed in order to describe the dynamics of the gas in which the discharge takes place. At present, calculations of streamer discharges are performed using quasi two-dimensional [1, 2], fully two-dimensional [3–5] and even three-dimensional [6] models. The dimensionality of the model is an important factor determining authenticity of results concerning the detailed structure of the discharge channel. At the same time, the usage of a relatively simple quasi two-dimensional model (known in the literature as 1.5-D model) allows one to describe discharge processes qualitatively and to study the main important properties that govern its development [7].

One of the non-obvious features of a streamer discharge is its ability to propagate in weak electric fields. A weak electric field is here defined as a field of some hundreds of kV m^{-1}, which is close to the field necessary for stable streamer propagation in air. This weak field is considerably lower than the critical electric field that is needed for streamer inception $E_{cr} = 3$ MV m^{-1}. If a positive voltage is applied to a gap with a divergent electric field (point-plane, rod-plane, etc), the streamer is initiated in the region with high field strength in the vicinity of the anode and when it propagates towards the cathode it enters a region with a weak electric field. As established experimentally [8, 9], the minimum field strength of a uniform background field needed for stable propagation of a cathode-directed streamer in an electrode gap from some centimetres [9] to some tens of centimetres [8, 10] is $E_b \approx 0.43$–0.5 MV m^{-1}. The value of E_b depends on many factors, in particular on the humidity and the ambient temperature [7, 10]. Moreover, at atmospheric pressure the streamer discharge is always observed as a number of filamentary channels even in short gaps [11]. It is obvious that this branching leads to a redistribution of the space-charge and also influences the conditions for streamer development.

The discharge development has been studied using various numerical models, but the main efforts in this area have been applied to investigate the structure of a streamer and the internal plasma chemical reactions taking place as it propagates in strong electric fields. Only a few studies have been devoted to discharge simulations in a weak electric field. The results of these studies gave a phenomenological explanation of processes observed in a propagating streamer but obtained discharge parameters did not agree with experimentally determined data. In [2], the development of a long streamer (∼500 mm) was considered. Steady discharge propagation was found in a background field of 0.80-–0.85 MV m^{-1}. This agrees well with another theoretical value, namely $E_b = 0.7$ MV m^{-1}, obtained in [12] when the propagation of the streamer was calculated by considering the energy balance at the streamer head. Both results show significant deviation from experimental data as presented above. Simulations performed for a gap length of 10 mm have shown the ability of the streamer to propagate in a weaker field [3, 13]. But it is difficult to relate the background field strength to the streamer properties in [3] because of the non-uniformity of the electric field. In [13], discharge propagation took place in a constant background field of 0.5 MV m^{-1}. In this case, the streamer only propagated about 6 mm after it was accelerated in the region of a strong electric field. Furthermore, the duration of the process of streamer propagation was about 7 ns. During this period of time, the losses of electrons due to attachment and recombination, which are the main cause of the decreasing of conductivity of the discharge channel and determining its propagating ability, were negligible. Thus, there is a lack of theoretical studies about the conditions required for streamer development in weak and uniform electric fields.

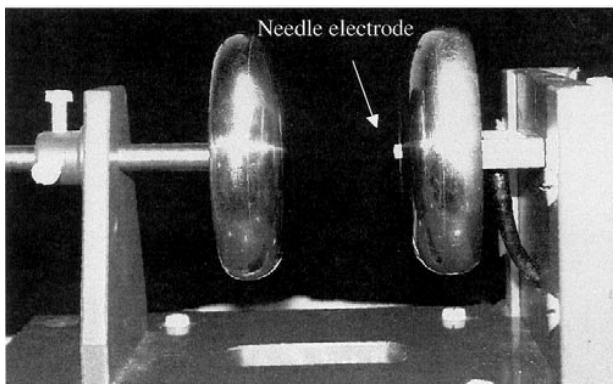

Figure 1. A photograph of the three-electrode system with the cathode to the left and with the anode and the trigger electrode to the right. The trigger needle electrode, together with its dielectric bushing, points out from the centre of the anode, as indicated by the arrow.

In this paper, the results of numerical simulations of positive streamers in air are presented. The simulations were performed for the conditions corresponding to recent published experiments [9, 11]. The experimental set-up is shown in figure 1, and consisted of a three-electrode arrangement. Two electrodes with a Rogowski profile provided a uniform background field. In a hole in the anode, a needle was inserted in order to trigger the streamer discharge. The needle was insulated from the anode. The gap length was 33 mm. The distributions of electrostatic fields were strongly non-uniform close to the needle tip. The field strength at the needle tip was about 20 MV m^{-1} but fell to a constant value a few millimetres from the tip. Thus, the streamer propagated about 30 mm in a weak and uniform background field after the initiation in the region of enhanced field near the anode. The experimental set-up included a measurement of the needle current, which gave the injected charge into the gap. A photographic film that was mounted on the cathode gave the number of streamer branches. With these two measurements, the charge per unit length of the streamer was estimated.

The structure of the paper is as follows. The mathematical model used and the method of calculation of the electric field in the electrode gap are described in section 2. The numerical results of streamer propagation at different values of the background electric field strength and a comparison with experimental results are presented in section 3. In section 4, energetic characteristics of a streamer propagating in a weak electric field (Joule dissipation, electric field energy) are analysed.

2. Mathematical model

2.1. Basic equations

In this study, a quasi two-dimensional model of the streamer was used. The streamer was considered as a cylindrical channel of fixed radius R_c. It was supposed that charge is distributed uniformly on the cross section of the channel. To model the principal behaviour of the discharge plasma, only one generic positive ion species and one generic negative ion species were included in the model. Hence, the detailed chemical kinetics of the discharge plasma was not considered. Ionic diffusion was not taken into account, as it does not play any significant role during the streamer propagation since the propagation lasts only for some hundreds of nanoseconds. Under these conditions, the system of continuity equations for densities of electrons, positive and negative ions was written in the following manner:

$$\begin{aligned}
&\frac{\partial n_e}{\partial t} + \operatorname{div}\left(n_e \vec{w}_e + D_e \nabla n_e\right) \\
&\quad = \alpha n_e |w_e| - a n_e |w_e| - \beta_{ep} n_e n_p + S_{ph} + S_0 \\
&\frac{\partial n_p}{\partial t} + \operatorname{div}\left(n_p \vec{w}_p\right) = \alpha n_e |w_e| - \beta_{ep} n_e n_p - \beta_{pn} n_p n_n + S_{ph} \\
&\frac{\partial n_n}{\partial t} + \operatorname{div}\left(n_n \vec{w}_n\right) = a n_e |w_e| - \beta_{np} n_p n_n
\end{aligned} \tag{1}$$

where t is the time; n_e, n_p, n_n are the number densities of electrons, positive ions and negative ions respectively; w_e, w_p, w_n are the drift velocities of electrons, positive ions and negative ions respectively; α is the ionization coefficient; a is the net attachment coefficient taking into account two- and three-body attachment of electrons to oxygen molecules; D_e is the diffusion coefficient for electrons; β_{ep}, β_{pn} are the coefficients of electron–ion and ion–ion recombinations respectively; S_{ph} is the rate of photoionization; S_0 is the rate of appearance of initial electrons (see below).

All coefficients in the system of equations (1) are functions of the local electric field strength obtained from the solution of the Poisson equation, which is written in the following form (cylindrical co-ordinates)

$$\begin{aligned}
&\frac{\partial^2 \varphi}{\partial z^2} + \frac{\partial^2 \varphi}{\partial r^2} + \frac{1}{r}\frac{\partial \varphi}{\partial r} = -R(z,r) \\
&E(z) = -\frac{\partial \varphi}{\partial z} \qquad E(r) = -\frac{\partial \varphi}{\partial r}
\end{aligned} \tag{2}$$

where $\varphi(z, r)$ is the potential; E is the electric field strength; z is the axial co-ordinate, with its origin at the cathode, along the symmetry axis of the electrode gap; r is the radial co-ordinate ($r = 0$ on the symmetry axis); $R(z, r)$ is the space-charge density, $R = e(n_p - n_e - n_n)/\varepsilon_0$ (e is the elementary charge; ε_0 is the dielectric constant).

The magnitudes of the rate coefficients and their dependences on the electric field were taken from [1] except the formulae for the attachment coefficient. The dependence $a(E)$ given in [14] was approximated by the power function $a/N = b(E/N)^c$ where $b = 1.5581 \times 10^{-36}$, $c = -1.0864$ for $E/N < 4 \times 10^{-16}$ V cm^2; $b = 1.0167 \times 10^{1}$, $c = 1.3024$ for $4 \times 10^{-16} < E/N \leqslant 1.5 \times 10^{-15}$ V cm^2; $b = 6.6466 \times 10^{-29}$, $c = -0.66589$ for $E/N > 1.5 \times 10^{-15}$ V cm^2 (N is the gas density).

The rate of ionization of oxygen molecules by absorption of photons that are radiated by excited molecules of nitrogen S_{ph} was calculated according to [15]

$$\begin{aligned}
S_{ph} = \frac{R_c^2}{4}\frac{P_T}{P_T + P}\frac{\omega\zeta}{\alpha}\frac{1}{\ln(\chi_2/\chi_1)}\int_0^{S_z} \alpha n_e |w_e| \\
\times \frac{\exp(-k_1|z - z_1|) - \exp(-k_2|z - z_1|)}{|z - z_1|^3}\,\mathrm{d}z
\end{aligned} \tag{3}$$

where P is the gas pressure; the parameter $P_T = 4$ kPa; the factor $\omega\zeta/\alpha = 1.1 \times 10^{-2}$; $\chi_1 = 0.026$ Pa^{-1} m^{-1}, $\chi_2 = 1.5$ Pa^{-1} m^{-1} are the cross sections of an absorption of radiation for frequencies ν_1 and ν_2 corresponding to the wavelengths of 102.5 nm and 98 nm, respectively; $k_{1,2} = \chi_{1,2} P_{O_2}$ are the absorption coefficients of radiation by oxygen molecules (P_{O_2} is the partial pressure of oxygen in air); $|z - z_1|$ is the axial distance between points of radiation and absorption of photons; S_z is the length of the discharge gap.

The channel radius was taken to be $R_c = 200$ μm. This value can be found as an average channel radius obtained by fully two-dimensional simulations [3, 4] and it is in agreement with available experimental data (a discussion regarding streamer radius can be found in [7]). The discharge current I was calculated using Sato's equation [16]

$$I = \frac{e\pi R_c^2}{U}\int_0^{S_z}\left(n_p w_p - n_e w_e - n_n w_n + D_e\frac{\partial n_e}{\partial z}\right)E_{st}\,\mathrm{d}z$$

where U is the applied voltage and E_{st} is the distribution of the axial component of the electrostatic field in the gap.

2.2. Boundary and initial conditions

The boundary conditions for the equation system (1) were the following. The density of positive ions on the anode surface was $n_p(S_z, t) = 0$ and the density of negative ions on the cathode surface was $n_n(0, t) = 0$. The boundary condition on the cathode for the electron density requires a special consideration. In the general case, it should include the production of secondary electrons by photons, positive ions and metastables. However, during the streamer propagation, all secondary electrons emitted from the cathode enter a weak electric field. Thus, they do not produce ionization and therefore do not contribute to discharge development. But secondary processes become significant at the streamer–cathode interaction, when the streamer head approaches the cathode. In order to obtain this effect qualitatively, the simplest boundary condition was used, taking into account a production of secondary electrons on the cathode due to impacts of positive

ions: $n_e(0,t) = \gamma n_p(0,t)\left|w_p(0,t)\right| / |w_e(0,t)|$ ($\gamma = 10^{-4}$ is the coefficient of secondary emission). The anode was considered as a perfectly absorbing boundary for electrons and the condition $n_e(S_z,t) = 0$ was used here. This condition describes the effect of the anode space-charge layer.

The commonly used approach to represent initial conditions for the equation system (1) is the assumption that a quasi-neutral layer or 'plasma spot' exists in the gap, which initiates the discharge [1, 3, 4]. This appears to be artificial because the location of charges and their densities are set arbitrarily. A more physical approach is presented in [17]. It is well known that the source of initial electrons is provided by collisional detachment from negative ions. In air at atmospheric conditions, the steady-state density of negative ions is about $n_{n0} = 10^9$ m^{-3} [18]. Following [17], it was assumed that O_3^- is the dominant type of negative ion. The rate of appearance of electrons due to detachment is

$$S_0 = \nu_{det} n_{n0} \tag{4}$$

where ν_{det} is the detachment frequency. The magnitude of ν_{det} is proportional to the frequency of elastic collisions ν_{el}

$$\nu_{det} = k\,\nu_{el}\exp\left(-W_l/W_{ch}\right). \tag{5}$$

Here $W_l = 3.29 \times 10^{-19}$ J (2.05 eV) is the electron affinity; $W_{ch} = 0.5 \times M \times (\mu_{n0} \times E)^2$ is the chaotic energy of the ions; $\mu_{n0} = 2.55 \times 10^{-4}$ m^2 V^{-1} s^{-1} is the mobility of the ions; $\nu_{el} = 0.79 \times 10^{10}$ s^{-1}; $M = 5.3 \times 10^{-20}$ kg is the mass of the ion; $k = 0.1$ is the similarity coefficient. As has been noted in [17], the term S_0 of the equation for electron density in the system (1) plays a role only in the initial stage of streamer inception in a strong electric field and a balance equation for O_3^- ions may be omitted. The magnitude of S_0, for example, at field strength $E = 20$ MV m^{-1}, which is typical for the streamer head, is $S_0 \sim 5 \times 10^{17}$ m^{-3} s^{-1} and is considerably lower than the magnitudes of other terms in the right-hand sides of equations (1).

The system of equations (1) was solved by the flux-corrected transport technique. The time step Δt was limited by the Courant criteria $c = \Delta t\,|w_e|/\Delta z$ (Δz is the space step). The spatial resolution was determined by the procedure of the electric field calculation, as described in the following section.

2.3. The calculation of the electric field

As mentioned, the streamer development was initiated in a small region of a strong divergent electric field with a coefficient of non-uniformity (which is the ratio of maximal field to the mean one) of about 30 and higher. The extension of the region with a non-uniform electric field was less than 5% of the gap length. Such conditions were typical for the experiments presented in [9, 11] where disc electrodes created a weak and uniform background electric field (figure 1). The local field enhancement took place close to the tip of the needle, which passed through a dielectric bushing placed in a hole in the centre of the anode. The presence of a dielectric material (the permittivity was $\varepsilon = 5$) gave additional field enhancement. In the numerical simulations, the real system of three electrodes was replaced by a two-electrode system 'protrusion on plate–plate' where the plate with a protrusion represented the anode + needle and the other plate represented the cathode. In such a system it was possible to maintain the level of the background uniform field and change field enhancement at the tip of the protrusion by changing its geometry. A hyperbolic shape was assigned to the protrusion and the geometric parameters of this were varied until we obtained a similar distribution of the electrostatic field as was obtained in the experimental electrode system. The 'protrusion on plate–plate' geometry requires a very fine axial and radial mesh in the anode region to accurately resolve the shape of protrusion. In the general case of a curved electrode, points of a finite-difference mesh do not lie on the boundary and the shape of the electrode is approximated in order to represent it in a boundary condition. A new meshing is needed each time if the configuration or the dimensions of the electrodes are changed. To simplify the meshing procedure, the problem was transformed into a rectangular computational domain with a uniform mesh. The main stages of the procedure are:

(i) transformation of the physical domain into a rectangular computational domain;
(ii) finding the potential distribution in the computational domain; and
(iii) obtaining the solution in the physical domain by back transformation.

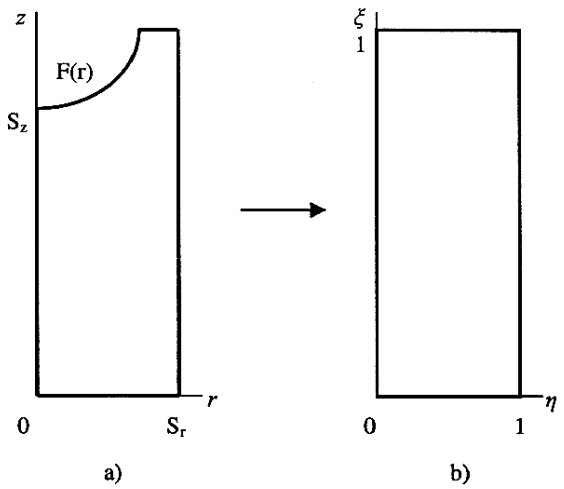

Figure 2. The physical domain (a) and the computational domain (b). The geometry function $F(r)$ defines the shape of the protrusion in the physical domain.

This approach is widely used in fluid mechanics [19] and was employed here for the electric field calculations. Let us consider a two-dimensional physical domain with a rotational symmetry of the electrode system including a curved electrode (figure 2(a)). The axial co-ordinate z has its origin at the lower boundary and it coincides with the symmetry axis where the radial co-ordinate r is equal to zero. S_z and S_r are the gap length and the radial dimension of the domain, respectively. In the physical domain, the axial and the radial distributions of the electric field E_z and E_r are found as the derivatives of the potential $\varphi(z,r)$ along corresponding directions, obtained from the solution of the Poisson equation (2). The physical domain is transformed into the rectangle $0 \leqslant \xi \leqslant 1, 0 \leqslant \eta \leqslant 1$ (figure 2(b)) using relations $\xi = z/f(r)$

Table 1. Definitions of the geometry function $F(r)$.

Electrode system	$F(r)$		Comments
Sphere–plate	$a - \left(a^2 - r^2\right)^{1/2}$		a is the radius of the sphere
Ellipse–plate	$a\left(1 - \left(1 - r^2/b^2\right)^{1/2}\right)$		a, b are semi-axes of the ellipse
Paraboloid–plate	$a(r^2/b^2)$		a is the height of the parabola $a = z(S_r) - S_z$; $b = S_r$
Hyperboloid–plate	$S_z\left(\left(1 + r^2/b^2\right)^{1/2} - 1\right)$		b is the imaginary semi-axis of the hyperbola
Protrusion of elliptic	$a\left(1 - \left(1 - r^2/b^2\right)^{1/2}\right)$	$r \leqslant b$	a, b are the height and the radius
shape on a plate–plate	a	$r > b$	of the base of the protrusion, respectively
Protrusion of parabolic	$a(r^2/b^2)$	$z < a + S_z$	a is the height of the protrusion;
shape on a plate–plate	a	$z \geqslant a + S_z$	b is the radius of the base of the protrusion
Protrusion of hyperbolic	$S_z\left(\left(1 + r^2/b^2\right)^{1/2} - 1\right)$	$z < a + S_z$	a is the height of the protrusion;
shape on a plate–plate	a	$z \geqslant a + S_z$	b is the imaginary semi-axis of the hyperbola

and $\eta = r/S_r$, where ξ and η are the axial and the radial co-ordinates in the computational domain; $f(r) = z_{\max} = S_z + F(r)$ is the geometry factor. Function $F(r)$ determines the shape of the upper boundary (some examples are shown in table 1). Equation (2) should also be transformed into the new co-ordinate system (ξ, η). Partial derivatives along the z and r directions are:

$$\frac{\partial^2\varphi}{\partial z^2} = \frac{1}{f^2(r)}\frac{\partial\varphi^2}{\partial\xi^2} \tag{6a}$$

$$\frac{\partial\varphi}{\partial r} = -\xi\frac{1}{f(r)}\frac{\partial f(r)}{\partial\eta}\frac{\partial\varphi}{\partial\xi} + \frac{\partial\varphi}{\partial\eta} \tag{6b}$$

$$\frac{\partial^2\varphi}{\partial r^2} = \left(\frac{1}{f(r)}\frac{\partial f(r)}{\partial\eta}\right)^2\xi^2\frac{\partial^2\varphi}{\partial\xi^2} + \frac{\partial^2\varphi}{\partial\eta^2} - \frac{2}{f(r)}\frac{\partial f(r)}{\partial\eta}\xi\frac{\partial^2\varphi}{\partial\eta\partial\xi} + \left[2\left(\frac{1}{f(r)}\frac{\partial f(r)}{\partial\eta}\right)^2 - \frac{1}{f(r)}\frac{\partial^2 f(r)}{\partial\eta^2}\right]\xi\frac{\partial\varphi}{\partial\xi}. \tag{6c}$$

By substituting (6) into (2) one gets the following equation for the potential distribution in the computational domain

$$C_{zz}\frac{\partial^2\varphi}{\partial\xi^2} + C_{zr}\frac{\partial^2\varphi}{\partial\xi\,\partial\eta} + C_{rr}\frac{\partial^2\varphi}{\partial\eta^2} + C_z\frac{\partial\varphi}{\partial\xi} + C_r\frac{\partial\varphi}{\partial\eta} = -R(\xi,\eta). \tag{7}$$

The coefficients in equation (7) are

$$C_{zz} = \frac{1}{f(r)^2} + \xi G^2 \qquad C_{zr} = -2\xi G/S_r \qquad C_{rr} = 1/S_r^2$$
$$C_z = \xi\left(G^2 - Q - G/\eta\right) \qquad C_r = 1/\eta\,S_r.$$

The parameters G and Q are determined by the geometrical factor $G = \mathrm{d}(\ln f(r))/\mathrm{d}r$; $Q = \mathrm{d}^2(\ln f(r))/\mathrm{d}r^2$. $R(\xi, \eta)$ in (7) is the space-charge density in co-ordinates (ξ, η).

Finally, the components of the electric field in the physical domain can be found as

$$E_z = -\frac{\partial\varphi}{\partial z} = -\frac{1}{f}\frac{\partial\varphi}{\partial\xi}$$
$$E_r = -\frac{\partial\varphi}{\partial r} = \xi G\frac{\partial\varphi}{\partial\xi} - \frac{1}{S_r}\frac{\partial\varphi}{\partial\eta}.$$

The boundary conditions for equation (7) were the potentials of electrodes $\varphi(0, \eta) = \varphi_c$ and $\varphi(1, \eta) = \varphi_a$. Both potentials were assumed to be step functions of time and were applied simultaneously. On the inner boundary, the symmetry boundary condition $\partial\varphi/\partial\eta = 0$ was used. On the outer boundary, a linear potential distribution was assigned. Equation (7) was solved by a multigrid method [20] on a uniform mesh. The electrostatic field distributions calculated for different configurations of electrodes were in close agreement with available analytical solutions and with the field distributions achieved by a finite-element solution of the Laplace equation [21].

The presented approach allowed us to perform calculations of electric fields in gaps with electrodes of complex geometry and to control field distributions in a wide range by changing the shape of the protrusion.

3. Results and discussion

3.1. Typical numerical results

Typical results obtained from the simulations are shown in figure 3 for the case of $E_b = 0.5$ MV m^{-1}, where the cathode is found to the left and the anode + needle is found to the right. The streamer inception took less than one nanosecond after voltage application. As can be seen in figure 3(*a*), the density of electrons increased during the formation stage up to about 10^{20} m^{-3} ($t = 1$ ns). It slightly decreased with time at the propagating streamer front, but in the streamer channel, particularly at the anode ($z > 30$ mm), it decreased about two times due to attachment and recombination. These regularities are observed in figure 3(*b*), where the evolution of plasma conductivity σ in the discharge channel is shown. At the streamer front, the magnitude of conductivity remains always constant and equal to about 0.23 S m^{-1} during propagation ($t = 4$–18 ns). In the anode region, it decreased around five times from about 4 S m^{-1} to about 0.8 S m^{-1}. The magnitude of the plasma conductivity in the streamer channel obtained from the simulations coincides well with known data [7].

According to the existing physical conception, the propagation of a positive streamer is maintained by photoionization at its front. Due to this process, secondary electron avalanches develop at the streamer head and add a positive space-charge to the discharge channel. The dynamics of the net charge under the considered conditions is shown in

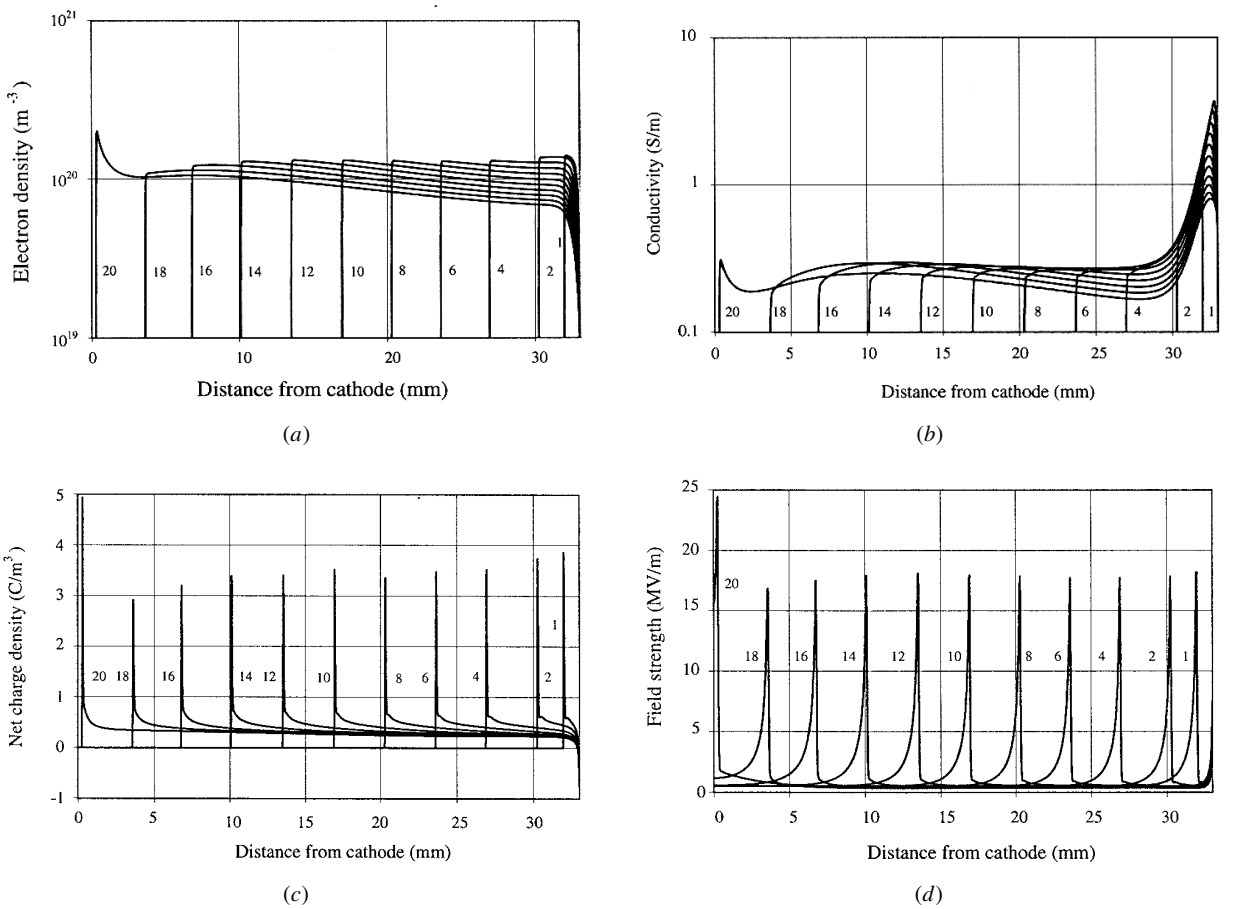

Figure 3. The temporal development of the distribution of selected plasma properties in the electrode gap during the streamer propagation. $z = 0$ at the cathode and $z = 33$ mm at the anode. The time for each profile is shown in nanoseconds. The background electric field is 0.5 MV m^{-1}. The parameters shown are: (*a*) electron density; (*b*) conductivity; (*c*) space-charge density; (*d*) electric field strength.

figure 3(*c*). It is notable here that since the streamer left the region with an enhanced electrostatic field and propagated in the uniform field $E_b = 0.5$ MV m^{-1} (curves for $t = 4$–14 ns), the maximum net charge at the streamer head was practically constant. The same behaviour was obtained for distribution of the electric field strength (figure 3(*d*)). This indicates a stable discharge propagation mode and the magnitude of the corresponding background field 0.5 MV m^{-1} is in agreement with known data.

When the streamer front approached the cathode region, a cathode–streamer interaction was observed. In this stage of discharge development, the maximum of the net charge slightly decreased (figure 3(*c*), curves for $t = 16$ and 18 ns) and then, when the streamer head arrived in the vicinity of the cathode, it increased rapidly (curve for $t = 20$ ns). A corresponding significant increase of the maximum of the electric field strength can be clearly seen in figure 3(*d*). This field enhancement produced intensive ionization and the increase of electron density and conductivity shown in figures 3(*a*) and 3(*b*), respectively. It has been established in [22] that these phenomena are conditioned by a release of electrostatic energy accumulated in a streamer channel–cathode system.

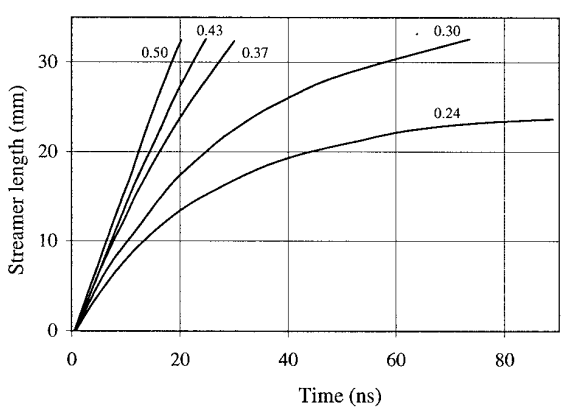

Figure 4. The streamer length over time for different background electric fields (shown in MV m^{-1}). $L_{st} = 0$ at the anode and $L_{st} = 33$ mm at the cathode.

3.2. Streamer parameters in a different background field

Six different values of the background electric field were considered: $E_b = 0.24$; 0.30; 0.345; 0.37; 0.43 and 0.50 MV m^{-1}. As was mentioned, the background field $E_b = 0.5$ MV m^{-1} was obtained from the simulations as the streamer stable propagation field. Due to this stability, the streamer length L_{st} increased linearly with time (figure 4).

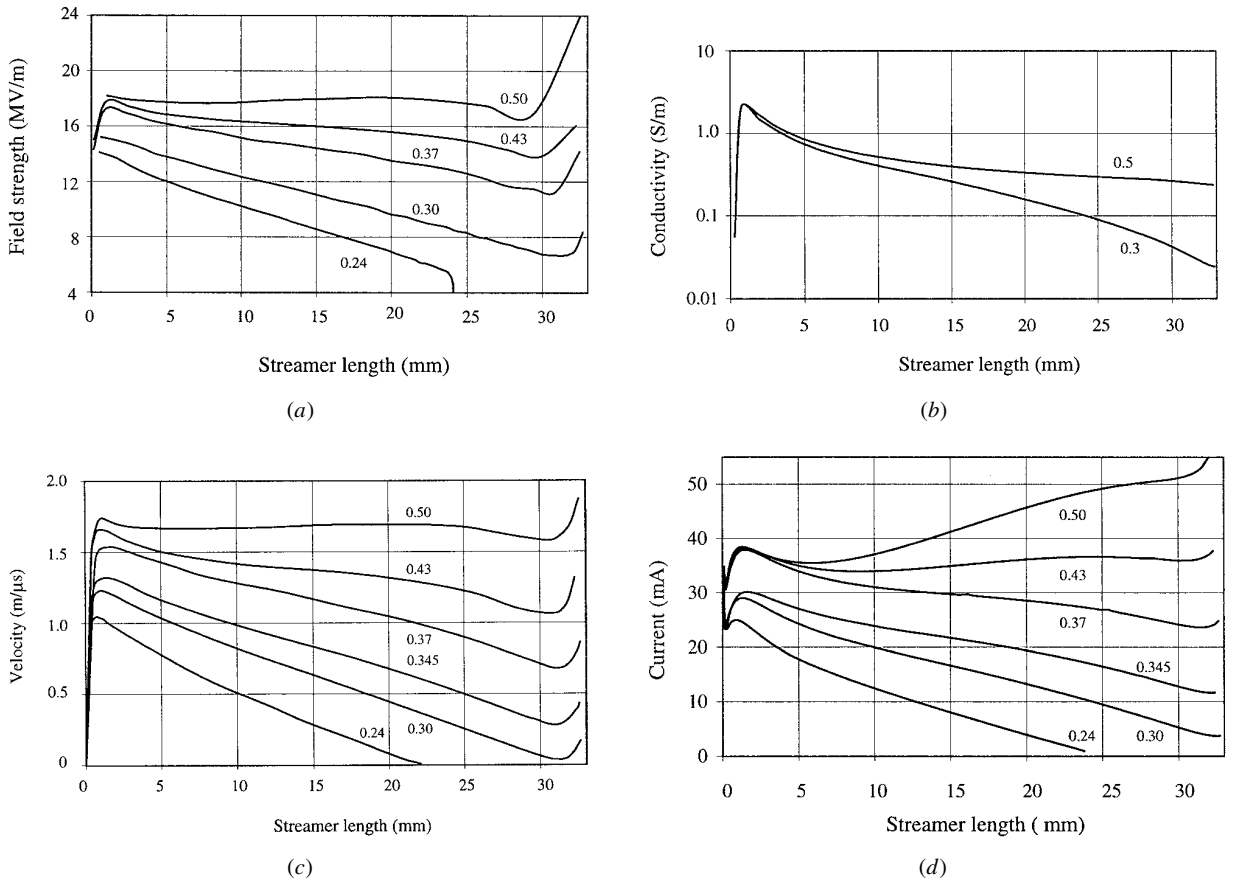

Figure 5. Parameters of the streamer propagating in a different background field (shown in MV m^{-1} at the curves): (*a*) electric field at the tip of the streamer; (*b*) average integral conductivity of the streamer channel; (*c*) streamer velocity; (*d*) discharge current.

The development of the channel length over time took a more and more logarithmic shape when decreasing the background electric field strength. At $E_b < 0.3$ MV m^{-1}, the streamer was not able to cross the gap. This critical value coincides well with the experimental observations where the minimum streamer crossing field was found to be around 0.29 MV m^{-1} [9].

Variations of streamer parameters with the increase of its length obtained in a different background field are shown in figure 5. During the stable streamer propagation in the field of 0.5 MV m^{-1}, the maximum field strength at its tip E_{max} was constant (figure 5(*a*)). In a lower background field, E_{max} decreased linearly with the increase of streamer length. When E_b was below the minimal crossing field, streamer termination took place in the middle of the gap and E_{max} decreased dramatically (curve for $E_b = 0.24$ MV m^{-1}). It is seen in figure 5(*a*) that the maximum field strength increased rapidly at small values of streamer length ($L_{st} < 2$ mm) and when streamer approached the cathode ($L_{st} > 28$ mm). The first rise was observed due to space-charge accumulation produced by the initial electrons in the initial strong field near the anode. In the other case, the reason of the field enhancement was a streamer–cathode interaction.

The results of the calculations also show that the parameters of the plasma channel behind the propagating streamer front depend on background field. The development of the average integral conductivity in the streamer channel is presented in figure 5(*b*) for the stability field 0.5 MV m^{-1} and for the minimal crossing field 0.3 MV m^{-1}. It can be seen that the conductivity of the plasma produced during the formation stage ($L_{st} < 2$ mm) was the same for both cases. But during propagation in different weak fields it was lower for lower E_b and the difference reached an order of magnitude when the streamer approached the cathode.

Since the intensity of photoionization and production of secondary electron avalanches needed for discharge front propagation are governed by the electric field at the streamer head, it is natural to expect that a variation of the streamer velocity W_{st} will follow the behaviour of E_{max}. As can be seen in figure 5(*c*), the streamer propagation at $E_b = 0.5$ MV m^{-1} took place with an almost constant velocity. In a lower background field, the velocity decreased with streamer length in the same linear manner as the field at its tip (figure 5(*a*)). Discharge front acceleration in the anode and in the cathode regions also corresponded to the increase of E_{max}. It is notable that streamer termination in the field $E_b = 0.24$ MV m^{-1} was observed when its velocity reached about 10^5 m s^{-1}. This value is in agreement with known data for minimum velocity of streamer propagation [15]. At the same time it is necessary to note that the magnitudes of W_{st} obtained in present simulations and shown in figure 5(*c*) are slightly overestimated in comparison with the results of fully two-dimensional simulations [13]. The reason is that a radial expansion of the discharge channel was not taken into account in the present model.

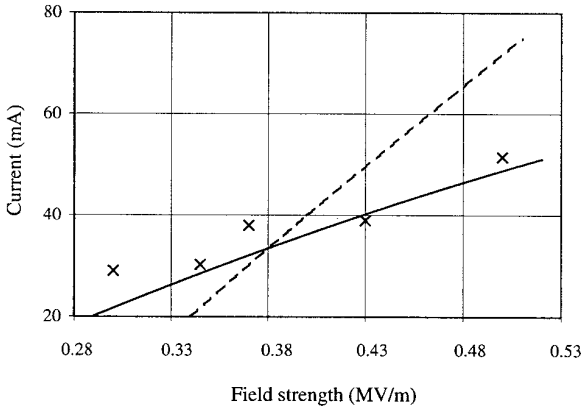

Figure 6. The amplitude of the discharge current: the solid curve represents the measured current on the needle; the dashed curve represents the measured current on the cathode. The points are the results obtained from simulations.

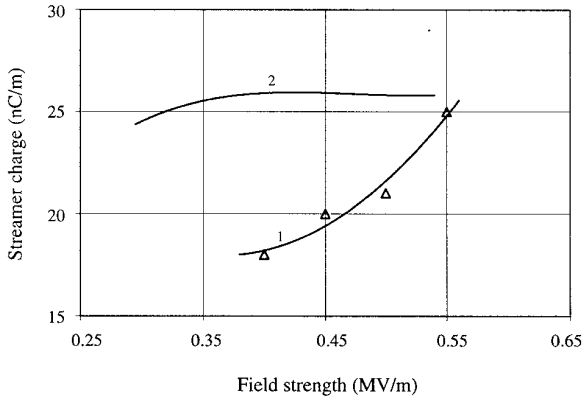

Figure 7. Streamer charge per unit of its length. Curve 1 is an interpolation curve of the experimental data [11]. Curve 2 represents the results of the simulations.

Streamer propagating in different background fields produces different currents in the external circuit (figure 5(*d*)). At least two common phenomena for different E_b can be recognized in the dependences of the current on streamer length at small lengths ($L_{st} < 3$ mm). The spike of the current at $L_{st} \sim 0.5$ mm is caused by the arrival of initial electrons, which appeared due to detachment from negative ions, to the anode. The amplitude of this spike is determined by the electrostatic field distribution in the vicinity of the protrusion and they were almost the same for the cases shown in figure 5(*d*). When the initial electrons approached the region with the enhanced field near the anode, they produced positive ions. To form a propagating ionizing wave (which a streamer is), the positive space-charge density must reach a certain magnitude. During the accumulation stage, the discharge current drops to the minimum seen in figure 5(*d*) at $L_{st} \sim 1$ mm. After the formation of the streamer, it starts to propagate. The maximum values of the discharge current at $L_{st} \sim 2$ mm are associated with the maximum of the streamer velocity shown in figure 5(*c*). It is interesting to note that the difference of ~20% between the maximum values of the velocity at $E_b = 0.37$ and 0.345 MV m^{-1} gives a corresponding ~20% difference in the current amplitudes. But, for $E_b = 0.37$, 0.43 and 0.50 MV m^{-1}, no difference in current behaviour at small streamer lengths was observed. When the streamer starts to enter into the region with a weak electric field ($L_{st} > 3$ mm), the current in the external circuit changed in a different manner depending on E_b. It grew at $E_b = 0.5$ MV m^{-1}, remained constant at $E_b = 0.43$ MV m^{-1} and decreased in a weaker electric field with the increase of the streamer length. When the streamer head approached the cathode region ($L_{st} > 30$ mm) the discharge current increased due to the streamer–cathode interaction. But this effect was only observed in the background fields $E_b = 0.37$, 0.43 and 0.5 MV m^{-1}.

A comparison of the maximum values of the discharge current obtained from the simulations and from the measurements [9] is shown in figure 6. The results of the experiments present amplitudes of the pure conductive current on a needle (solid curve) and the current measured on the cathode (broken curve) which includes both, conductive and induced, currents. As can be seen, the results of the simulations are closer to the results obtained for the pure conductive current.

A quantitative comparison between the experimental data presented in [11] and the simulations is presented in figure 7. The figure shows the mean linear charge density in one single streamer filament. The agreement is very good for a high background electric field, but deviates slightly for lower fields. Since the calculation is based on a volume integration of the space-charge density, the influence of the assigned streamer radius is significant. Using the radius as a varying parameter, it would be possible to match experiments with simulations. But because of a lack of experimental data on the relationship between the streamer radius and the background field, such a parameter matching was not pursued.

4. Energetic parameters of a streamer in a weak electric field

From an energetic point of view, the streamer inception and propagation are governed by the electrostatic energy accumulated in the electrode system. The density of the electrostatic energy $q = \varepsilon_0 E^2/2$ is determined by the spatial distribution of the electric field. The integration of this expression over the volume of the electrode gap gives the electrostatic energy Q accumulated in the system. Assuming a fixed radius (cross section) of the discharge channel and varying the upper limit of integration along the axial direction, one could calculate the distribution of electrostatic energy at different stages of streamer development. The results obtained in such a way are shown in figures 8(*a*) and 8(*b*) for values of $E_b = 0.5$ and 0.3 MV m^{-1}, respectively. The distribution of the electrostatic energy of the Laplacian field (that is, before any discharge) is presented by curves for the time equal to zero. A significant difference in the magnitudes of Q can be seen for $t = 0$ and 1 ns. This energy is spent for streamer formation and is practically the same for both cases. But the variation of the electrostatic energy during the streamer propagation differs. The stable propagation in the background field 0.5 MV m^{-1} is associated by a slight increase of the electrostatic energy (figure 8(*a*)). In contrast to this, the streamer loses energy if

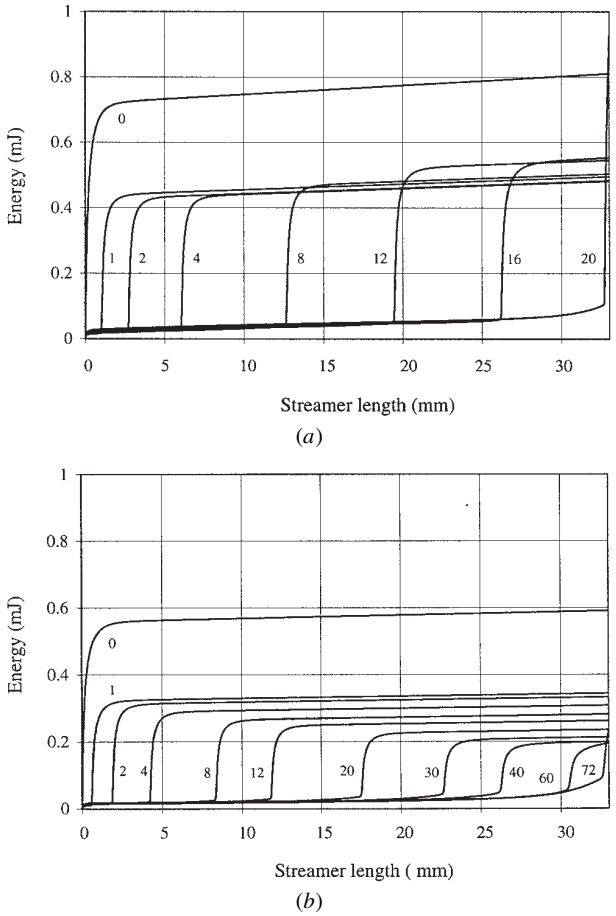

Figure 8. The electrostatic energy of streamer propagating in the field 0.5 MV m^{-1} (*a*) and 0.3 MV m^{-1} (*b*). Time is shown in nanoseconds.

the propagation takes place in the minimum streamer-crossing field 0.3 MV m^{-1} (figure 8(*b*)). A consequence of this behaviour is that the amount of electrostatic energy which can be released at the streamer arrival at the cathode, is significantly lower (about five times) in the last case (figure 8(*a*), $t = 20$ ns; figure 8(*b*), $t = 72$ ns).

The electrostatic energy in the plasma front is spent in inelastic collisions (excitation and ionization) and is carried away by radiation and Joule dissipation. The Joule dissipation JE due to flowing current (J is the current density) is the main part of the energy loss in a discharge and it also depends on the conditions for streamer development. As was obtained from the simulations, the magnitudes of JE remain constant in the case of background field $E_b = 0.5$ MV m^{-1} (figure 9) except in the vicinity of the electrodes. If $E_b = 0.3$ MV m^{-1}, then the Joule dissipation associated with the streamer head decrease with streamer length by three orders of magnitude. Dependences obtained for intermediate values of E_b showed a reduction of losses in the same manner as at 0.3 MV m^{-1} but the differences in magnitudes in the anode and cathode regions were not so significant.

5. Conclusions

The analysis of the results obtained from numerical simulations of streamer development in weak and uniform electric fields

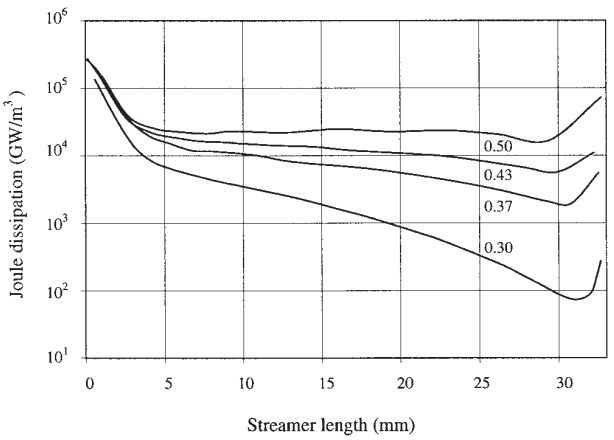

Figure 9. The Joule dissipation associated with the streamer head in different background fields.

showed that stable streamer propagation took place at a background electric field strength of 0.5 MV m^{-1}. At the same time, it was established that a streamer was able to cross an electrode gap of 33 mm length in a background field of 0.3 MV m^{-1}. Both these values agree well with experimental observations. During the stable streamer propagation, the internal parameters of the streamer channel (electron density, plasma conductivity and electric field at the front) remain practically constant. In background fields lower than 0.5 MV m^{-1}, the streamer velocity and the electric field at the streamer front decreased linearly with increased streamer length. It was shown that the discharge propagation in the stability field was associated with an increase of electrostatic energy at the streamer front. In contrast to this, the discharge front energy decreased if the streamer developed in a weaker electric field. This behaviour was accompanied by constant Joule dissipation at 0.5 MV m^{-1} and decreasing energy losses at the streamer front in a weaker background electric field.

References

[1] Morrow R and Lowke J J 1997 Streamer propagation in air *J. Phys. D: Appl. Phys.* **30** 614–27
[2] Aleksandrov N L and Bazelyan E M 1996 Simulation of long-streamer in air at atmospheric pressure *J. Phys. D: Appl. Phys.* **29** 740–52
[3] Kulikovsky A A 1998 Positive streamer in a weak field in air: A moving avalanche-to-streamer transition *Phys. Rev.* E **56** 7066–74
[4] Babaeva N Yu and Naidis G V 1996 Two-dimensional modelling of positive streamer dynamics in non-uniform electric field in air *J. Phys. D: Appl. Phys.* **29** 2423–31
[5] Georghiou G E, Morrow R and Metaxas A C 2000 Two-dimensional simulation of streamers using the FE-FCT algorithm *J. Phys. D: Appl. Phys.* **33** L27–L32
[6] Kulikovsky A A 1998 Three-dimensional simulation of a positive streamer in air near curved anode *Phys. Lett.* A **245** 445–52
[7] Bazelyan E M and Raizer Yu P 1998 *Spark Discharge* (Boca Raton, FL: CRC Press) p 295
[8] Allen N L and Ghaffar A 1995 The conditions required for the propagation of a cathode-directed positive streamer in air *J. Phys. D: Appl. Phys.* **28** 331–7
[9] Gao L, Larsson A, Cooray V and Scuka V 1999 Simulation of streamer discharges as finitely conducting channels *IEEE Trans. Dielectr. Electr. Insul.* **6** 35–42

[10] Allen N L and Boutlendj M 1991 Study of the electric fields required for streamer propagation in humid air *IEE Proc.* A **138** 37–43
[11] Gao L, Akyuz M, Larsson A, Cooray V and Scuka V 2000 Measurement of the positive streamer charge *J. Phys. D: Appl. Phys.* **33** 1861–5
[12] Gallimberti I 1972 A computer model for streamer propagation *J. Phys. D: Appl. Phys.* **5** 2179–89
[13] Babaeva N Yu and Naidis G V 1996 Simulation of positive streamers in air in weak uniform electric field *Phys. Lett.* A **215** 187–90
[14] Lowke J J and Morrow R 1995 Theoretical analysis of removal of oxides of sulfur and nitrogen in pulsed operation of electrostatic precipitators *IEEE Trans. Plasma Sci.* **23** 661–71
[15] Bazelyan E M and Razhanski I M 1988 *Spark Discharge in Air* (Novosibirsk: Nauka) p 165 (in Russian)
[16] Morrow R and Sato N 1999 The discharge current induced by the motion of charged particles in time-depended electric fields; Sato's equation extended *J. Phys. D: Appl. Phys.* **32** L20–L22
[17] Diyakov A F, Bobrov Yu K and Yurgelenas Yu V 1998 *Simulation of Positive Streamer in Air in Non-uniform Electric Field in Physics and Physics and Technology of Electric Power Transmission* (Moscow: MPEI Publishers) p 328 (in Russian)
[18] Raizer Yu P 1987 *Gas Discharge Physics* (Moscow: Nauka) p 592 (in Russian)
[19] Anderson D A, Tannehill J C and Pletcher R H 1990 *Computational Fluid Mechanics and Heat Transfer* (Moscow: Nauka) (Russian translation)
[20] 1998 MUDPACK 4.0 (University Corporation for Atmospheric Research, USA)
[21] Serdyuk Yu V and Gubanski S M 2000 Electric field calculation in gas discharge using domain transformation technique *Proc. Hakone VII, Int. Symp. on High Pressure Low Temperature Plasma Chemistry (Germany)* pp 129–33
[22] Odrobina I and Cernak M 1995 Numerical simulation of streamer–cathode interaction *J. Appl. Phys.* **78** 3635–42